Assessing the Palaeoenvironment Conditions of Perhistoric with Emphasis on the Drainage Network: Case Study of Tal-e Malyan (Anshan), Fars, Iran

Asghar Navidfar[*,1] ; Mehran Maghsoudi[1] ;Razyeh Lak[2] ;Alireza Sardari[3] ;
Masoud Rahimi[4] and Seyed Mohammad Zamanzadeh[1]

[*]Corresponding Author, 1Department of Geography, University of Tehran, Tehran, Iran.
E- mail:navidfar32@ut.ac.ir
[2]Department of Geology, Research Institute for Earth Sciences, Geological Survey of Iran, Tehran, Iran.
[3]Iranian Center for Archaeological Research (ICAR), Tehran, Iran.
[4]Department of Geography, Ferdowsi University of Mashhad, Mashhad, Iran.

Received: 0/0/0; Received in Revised form: 0/0/0; Accepted: 0/0/0; Published: 0/0/0

Abstract

Tal-e Malyan, also known as Ancient Anshan, has been recognised as an archaeological site since at least the mid-nineteenth century. Covering an area of about 200 hectares, it was one of the major prehistoric centres and the capital of the Elamite civilisation during the 3rd and 2nd millennia BCE. This study provides a multi-proxy reconstruction of the palaeoenvironmental dynamics between 6000 and 3500 BP. By integrating sedimentological, geomorphological, and geoelectrical (Electrical Resistance Tomography, ERT) datasets with stratigraphic evidence from existing archaeological trenches in the Kur River Basin (Fars, Iran), we evaluate the environmental precursors to urban development. A total of 140 sediment samples were subjected to granulometric analysis to delineate depositional energy regimes. Additionally, ten geophysical profiles were surveyed to a depth of 20 m. The geoelectrical data identified a substantial palaeochannel conduit near Trench 18, measuring 20 m in width and 6 m in depth, dating to ca. 6000 BP, along with a secondary southern channel that is 5 m wide and 2 m deep. Furthermore, fluvial successions documented in Trench 8 suggest that two primary fluvial branches, originating from the western Qalat Mountains, intersected the site. These findings, supported by the presence of a lake environment on the eastern periphery, indicate that the spatial evolution and eventual relocation of settlements within the Beyza Plain were fundamentally governed by shifting hydro-geomorphological conditions and the need for stable water access.
Keywords: Ancient Sites, Drainage Network, Geoelectric, Tal-e Malyan (Anshan)

Introduction

Every problem in archaeology often leads to new questions in geoarchaeology (Renfrew, 1972). Interdisciplinary studies between archaeology and geomorphology, utilising a geoarchaeological approach, provide valuable insights into human-environment interactions in the past (Dong et al., 2024; Nehybaková et al., 2023; Emmanuel et al., 2017; Reynard et al., 2017; Pelfini et al., 2021). Geoarchaeologists strive to determine the transformations in the region, as well as the development and deterioration of sites in response to changes in palaeoenvironmental conditions (Chandel et al., 2022; Herrera-Franco et al., 2022; Prabhakar and Radhika, 2022; Xu and Wu, 2022; Quesada-Valverde and Quesada-Román, 2023) and catastrophic natural events that may have abruptly destroyed cultures and civilisations in the region (Waters, 1988; Gillmore et al., 2011; Woodward and Huckleberry, 2011; Maurizio and Silvestro, 2012; Ghilardi et al., 2013; Liritzis et al., 2019). The distribution of existing landforms and geomorphological processes are among the most significant criteria influencing the dispersion of human settlements during the recent Quaternary period (Lü et al., 2019; Persico et al., 2018; Aucelli et al., 2020; Brandolini and Carrer, 2021). Gradually, the human factor becomes increasingly significant in reconstructing landforms and influencing surface geomorphic processes (Jefferson et al., 2013; Tarolli et al., 2018; Goudie, 2020; Aguilar et al., 2020; Gibbard et al., 2022). The history of geoarchaeology encompasses not only the application of earth science methods to archaeology but also the long-term study of interactions between humans and the

natural systems dominant in a region (Hill and Rapp, 2014: 3008). In this regard, geoarchaeological and geotechnical methods (Bevan and Smekalova, 2013; Hatswell et al., 2025; Adameková et al., 2025) provide a wide range of strategies for studying ancient sites, saving time and costs while reducing the potential for destruction (Zielhofer et al., 2018).

Geoarchaeological studies in Iran began in the 1970s, focusing initially on Palaeolithic excavations and the systematic use of earth science methods to describe ancient details in caves and rock shelters (Taheri et al., 2007: 3341). In recent years, geoarchaeological studies have employed various methods and techniques based on landforms (Figure 1). Some notable studies include Geomorphology and sedimentology (e.g Maghsoudi et al, 2014: 1; Gillmore et al., 2011: 49; Biglari et al., 2015: 7; Heydari-Guran et al., 2021: 124; Kharazian et al., 2022), Geomorphology and climatic changes (Naderi Beni et al., 2025), Geophysics (e.g Aminpour., 2001: 4; Mofidi-Nasrabadi and Mirzaei., 2013: 89; Mohammadkhani and Naif., 2018: 1), and Soil micromorphology (e.g Khodabakhshi et al., 2012: 2; Maghsoudi et al., 2015: 1).

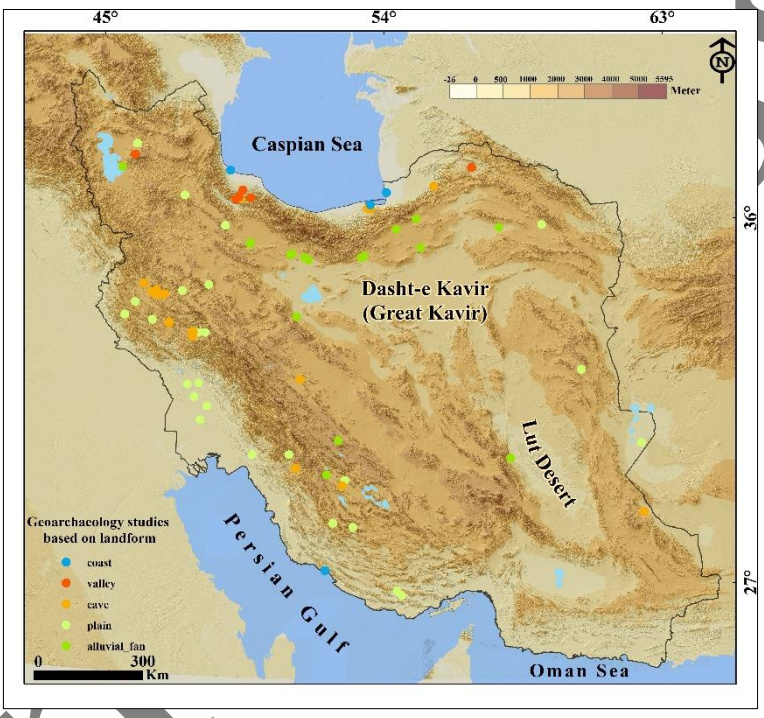

Figure 1: Map of Geoarchaeology study in Iran up to 2025.

Tal-e Malyan, an urban centre exceeding 200 hectares in the Iranian highlands, has a developmental trajectory characterised by four primary occupational phases: the Banesh Phase (Proto-Elamite: 5200–4600 BP), the Kaftari Phase (Old Elamite: 4200–3600 BP), the Qaleh Phase (Middle Elamite: 3300–3000 BP), and a later Sasanian reoccupation (ca. 1600 BP) (Sumner, 2003). Fundamental studies conducted in this region include: “Cultural Development and Settlement Patterns in the Kur River Basin” (Sumner, 1972: 155), “Economy and Environment of Malyan” (Miller, 1982), “Urbanism and Animal Exploitation in Southwest Highland Iran” (Zeder, 1985), “Mineralogical and Chemical Analysis of Banesh Period Ceramics” (Blackman, 1981), “Regional Economic Organisation in Banesh Period” (Alden, 1979: 207), “Spatial/Functional Analysis of Late Fourth Millennium Occupation” (Nicholas, 1980: 61), and “Proto-Elamite Texts from Tal-e Malyan” (Stolper, 1985).

Primarily, the significance of the Tel- e Malyan site, compared to other sites in the Kur River basin, lies in its vast size, prominence, and its continuous occupation across various periods (Banish Phase, Kaftari Phase, Qaleh Phase, and Sasanid, etc.). Additionally, its importance as a major city during the Middle Elamite period further underscores its historical and archaeological value. According to Sumner’s studies, no other sites within the Kuh River basin from the Banish Phase match the scale and size of Tel-e Malyan. Although numerous studies have been conducted at Tal-e Malyan, regarded

as an ancient city and one of the capitals of the Elamite civilisation in southwestern Iran, they have notably lacked geomorphological investigations.

This study aims to clarify the underlying factors that led to the establishment of the Tal-e Malyan (Anshan) site within the Kur River Basin and the Beyza Plain, with a particular emphasis on environmental and geomorphological controls. To achieve this goal, the research investigates the dominant geomorphological landforms and processes that have shaped the region and influenced human settlement patterns. Additionally, the research explores the function of the extensive wall and fortification system surrounding Anshan, seeking to explain its original purpose and the differential preservation of its various segments in relation to geomorphological processes and environmental dynamics.

The research aims to address the following questions posed by the archaeological team:

١. What factors contributed to the settlement of the Tal-e Malyan site in the Kur River Basin and the Beyza plain?
٢. What geomorphological forms and processes have existed in this area?
٣. What were the environmental conditions before and after the settlement at this site, and what is the sequence of these changes?
٤. From which sub-basins does the drainage network, not mentioned in the excavation reports, originate, and what impact did it have on the site?
٥. What was the function of the large wall and fortification surrounding Anshan (Tal-e Malyan), and why have some sections of this wall survived while others have been destroyed?

Study area

The Kur River basin, covering an area of 8,117 km² and with an average elevation of 2,600 m, is situated in Fars Province. Originating from the heights of Eqlid, the Kur River flows into Marvdasht through Tang-e Boraq. The river spans a total length of 280 km to Bakhtegan Lake (1:25,000 map by the Iran National Cartographic Centre).

The Ancient site of Tal-e Malyan lies within the Beyza Plain of the Kur River Basin, approximately 45 km northwest of Shiraz (Fig.2). Enclosed by extensive fortifications, the site covers around 200 hectares (Abdi, 1999). After its initial documentation by Sumner in 1968, the discovery of diagnostic brick fragments facilitated the identification of Malyan as ancient Anshan, a prominent capital of the Elamite civilisation (Reiner, 1973; Sumner, 2003). Chronologically dated to around 5,200 BP, the urban centre was enclosed by a monumental mud-brick wall, which measured 5 m in height and 10 m in width.

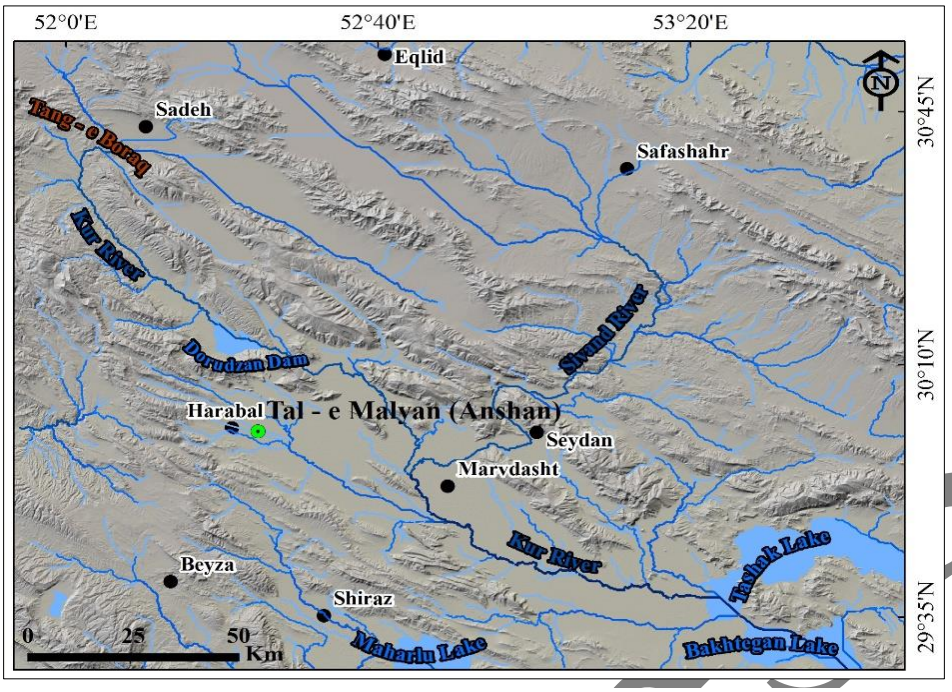

Figure 2: Geographical location of the study area (Hillshade map of SRTM DEM 30m)

The study area is situated within the Zagros Fold-and-Thrust Belt. In the Fars region, tectonic deformation is characterised by relatively gentle and open folding, predominantly manifesting as symmetric synclines and simple anticlines (Alaei Taleghani, 2017). The geomorphological mapping of the area reveals a diverse range of landforms, classified and illustrated in Table 1 and Figure 3, respectively:

Table 1: Zone of Landform in the study area.

Zone	Area (km^2)	Covers (percent)	Average height (m)	Average slope (degrees)
Mountain	1022	46.8	2341	20
Hill	29	1.33	1885	7.5
Pediment	93.87	4.3	1776	5.4
Alluvial plain	37.24	37.24	1786	3.9
Floodplain	30.59	1.4	1672	5.4
Alluvial fan	55.54	2.54	1771	5.14
Mountain plain	71.63	3.28	2115	6.34
Salty	25.92	1.18	1588	4.56
Closed depression	11.45	0.52	1597	5.25

The Mountainous Zone, encompassing 1,022 km² (46.8% of the study area), has a mean elevation of 2,341 m and an average gradient of 20° (Fig.3). The Hilly Zone constitutes a smaller physiographic unit, covering 29 km² (1.33%) with a mean elevation of 1,885 m and a slope of 7.5°. Situated at the interface between the plains and the mountainous uplands, the Pediment Zone (93.87 km²) occurs at the base of eroded anticlines and synclines, exhibiting an average elevation of 1,776 m with a slope of 5.4°. The Alluvial Plain, the second-largest geomorphological unit, accounts for 37.24% of the landscape, with a mean elevation of 1,786 m and a gentle gradient of 3.9°. The Floodplain Zone, which Flanks the Kur River, comprises 1.4% of the area, following a NW-SE trajectory with a mean elevation of 1,672 m and a slope of 5.4°. Alluvial Fans, making up 2.54% of the area, are predominantly located along the northern boundaries and the western reliefs of the Dorudzan Dam. Furthermore, Intermontane Plains (3.28%) are situated among the western reliefs at an average elevation of 2,115 m. Finally, interconnected depressions, which were inundated during past pluvial periods, are identified as Closed Saline Depressions (playas). These features are located within the lowlands downstream of the dam (Fig.3).

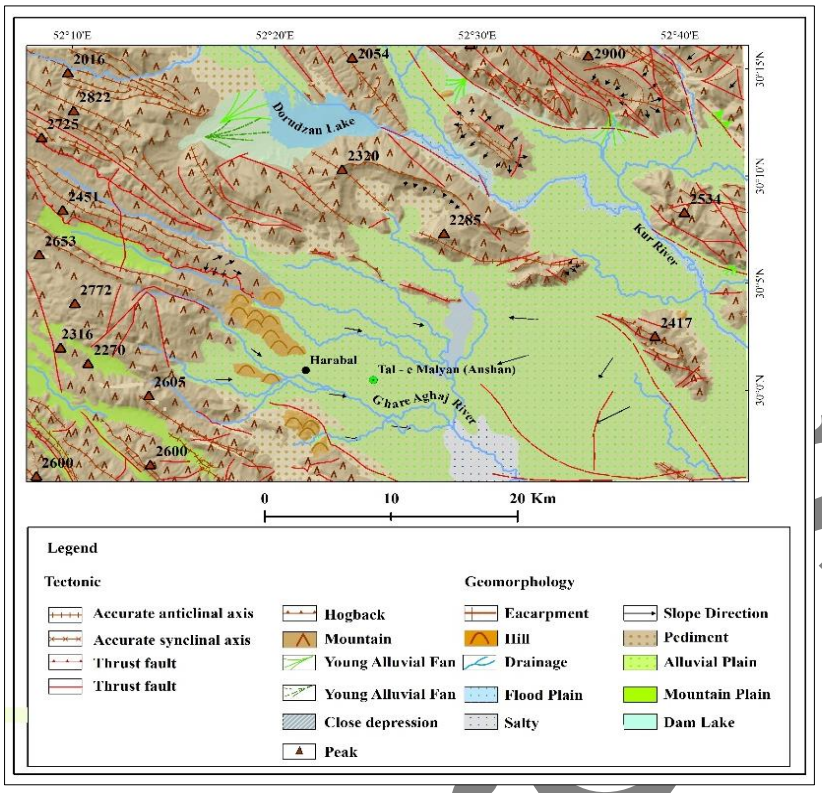

Figure 3: Geomorphology map of the study area (After: Sentinel 2 image - 20/07/2024)

Materials and Method

The systematic evaluation of the ancient sites was conducted across several strategic phases by archaeologists. The initial phase comprised a comprehensive site survey and the delimitation of core and buffer zones to establish the site's legal and archaeological boundaries. This procedure was executed for Tal-e Malyan (Anshan) under the auspices of the Iranian Centre for Archaeological Research (ICAR) in April 2017 (Sardari et al., 2019). A total of 22 stratigraphic trenches, measuring 2×2, 2×1, and 1×1 m, were excavated to a maximum depth of 4 m to evaluate the subsurface archaeological horizons (Fig.4).

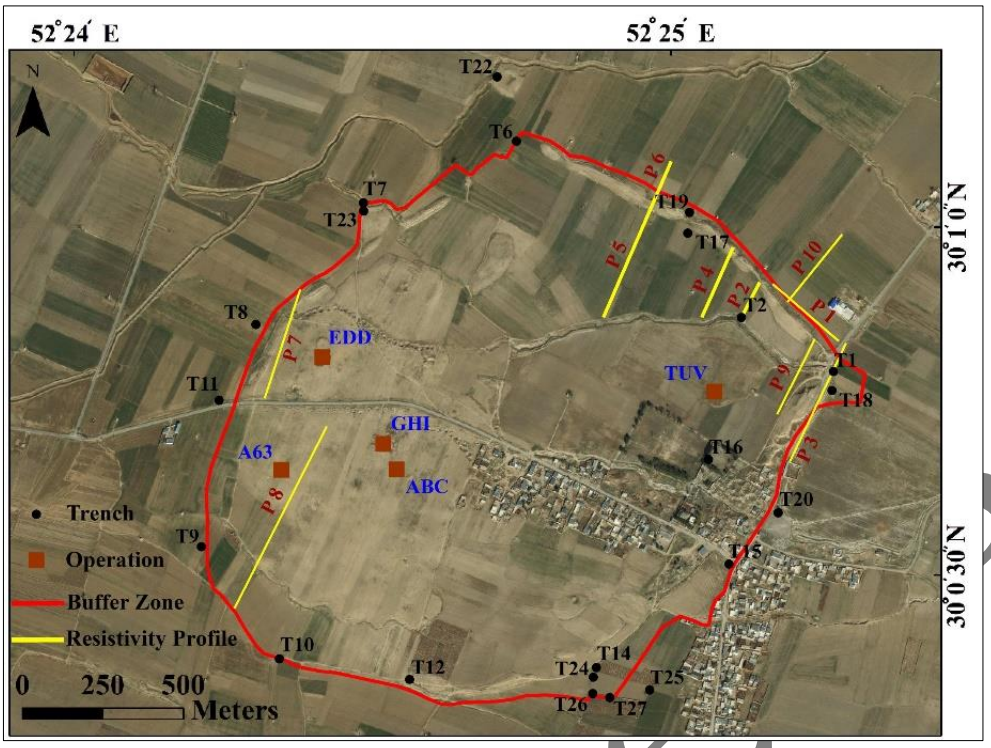

Figure 4: Buffer Zone, Resistivity Profile and Trenches of Tal-e Malyan, along with the location of the excavation operations conducted between 1971 – 2003 (For more information, see Sumner, W. M, 2003) (After: Google Earth 15/06/2024)

Texture of Sediments

The investigation of sedimentary texture involves analysing grain fabric, size distribution, morphology, and surface micro-texture. These parameters serve as critical indicators of textural maturity and depositional energy (Tucker, 2003; Lowe & Walker, 2014). Given the site's topographic position within the plain and its proximity to drainage networks originating from the western highlands, the landscape has been intermittently reshaped by fluvial dynamics. Although the sedimentary matrix is predominantly fine-grained, specific transects exhibit coarse-grained lithofacies indicative of high-energy channel deposits. The stratigraphic profile at Tal-e Malyan reveals a cultural sequence approximately 11 m thick. In the elevated western and southern sectors, both basal and terminal units are characterised by a fine-grained, sandy mud texture. In contrast, the eastern and northeastern sectors exhibit a tripartite stratigraphy: an 8-m-thick upper unit composed of fluvial successions over lower units of fine-grained alluvial plain facies. These basal layers grade into lacustrine deposits (lake sediments) associated with the endorheic (closed) depression to the east of the site (Fig.5).

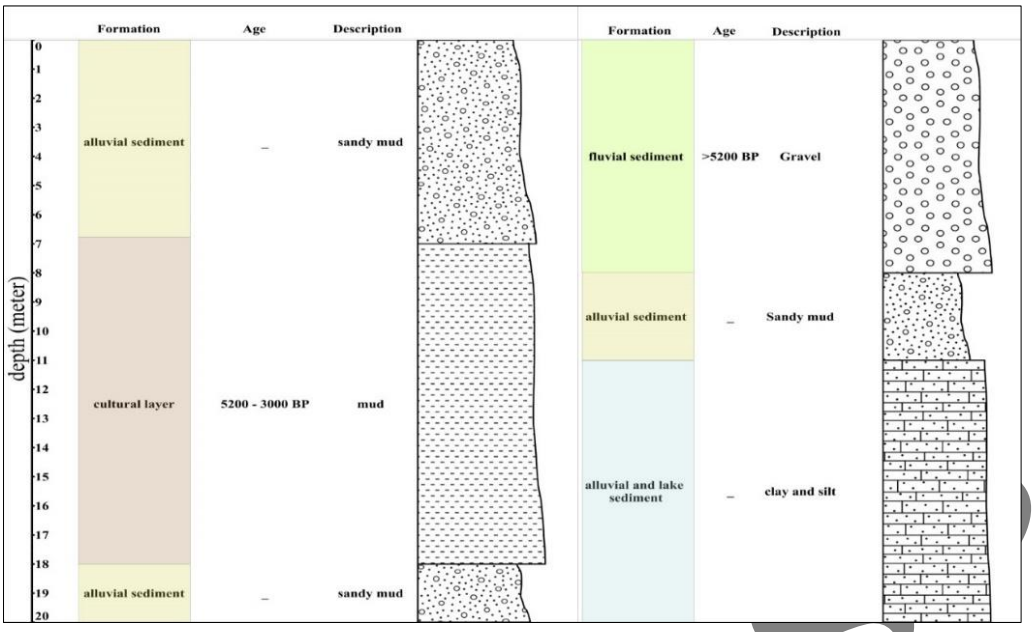

Figure 5: Lithostratigraphy of Tal-e Malyan.

To reconstruct the palaeoenvironmental conditions at the site, 140 sediment samples were systematically collected from the excavated trenches. The sampling strategy was based on observable lithological variations, including shifts in stratigraphic horizons, Munsell colour properties, textural transitions, and other diagnostic macromorphological characteristics (Fig.6).

Figure 6: a, b: preparing electrodes for geoelectrical study (depth of the geoelectrical study is 20m) – c: Sample collection was based on sedimentary layer changes, d: Sampling was conducted based on regular intervals. (After:10/06/2022).

To characterise the sedimentary texture, the samples were oven-dried at 105 °C for 24 hours to ensure complete moisture removal. The coarse fraction, comprising particles larger than 2 mm in diameter, was subsequently isolated from the gravellous and sandy matrices via mechanical sieving, following the Wentworth scale for clastic sediments. To sieve particles larger than 63 microns, 100 grams of each sample were selected for analysis. The samples were sieved for 15 minutes at 60% power. After

this process, the remaining sediments on the sieves were weighed, and their weight percentages were calculated. The hydrometer method[1] was used to determine the size distribution of soil and sediment particles smaller than 2 mm, especially in samples that were not completely dispersed (Gee and Bauder, 1986).

To sieve particles larger than 63 microns, 100 grams of each sample were selected for analysis. The samples were sieved for 15 minutes at 60% power. Next, the remaining sediments on the sieves were weighed, and their weight percentages were calculated.

The procedure for measuring particle diameter using the 152H hydrometer was as follows:

١. Weigh 50 grams of air-dried soil that has passed through a 2-mm sieve.
٢. Add 250 ml of distilled water and 100 ml of a sodium hexametaphosphate solution (50 g/l) to the soil sample.
٣. Allow 24 hours for sample preparation, then transfer the samples to 1000 ml graduated cylinders and dilute to the mark with distilled water.
٤. Measure hydrometer readings at specified time intervals.

The percentage of remaining soil in the graduated cylinder is calculated when the hydrometer measures the density of the mixture using the following formula:

١. $P=(R_a/W)\times ١٠٠$

Where:

P: Percentage of remaining soil in the graduated cylinder at the time of measurement,
R: Hydrometer reading recorded after applying the composite correction,
W: Weight of the soil sample used in the experiment.

The particle size of the soil was calculated using the following equation:

٢. $D=K\sqrt{L/T}$

Where:

L: Effective depth in centimetres.
T: Time from the initiation of soil sedimentation to the reading, measured in minutes.
K: Viscosity coefficient of the suspension.

Geoelectric Survey

To delineate the buried paleochannels within the site, a geoelectrical survey was conducted employing a dipole-dipole array configuration with a constant electrode spacing of 5 m (Fig.5). In this electrode geometry, the current (A, B) and potential (M, N) dipoles are collinear and maintained at an equal length (AB = MN = a). During the data acquisition, the potential dipole (MN) is incrementally displaced along the profile relative to a fixed current dipole (AB). The separation between the proximal current and potential electrodes is defined as na, where n represents an integer multiple (n = 1, 2, 3, ...). The effective investigation depth is approximated as (n+1)a/2. Apparent resistivity values are systematically assigned to the intersection point of two 45° vectors originating from the midpoints of the AB and MN dipoles. This methodology facilitates the construction of a 2D apparent resistivity pseudosection, providing a high-resolution vertical cross-section of the subsurface electrical properties along the established transect (Samadi, 2012) (Fig.7).

[1] The calculations of the hydrometer readings were performed according to the ASTM D422- 63 Standard.

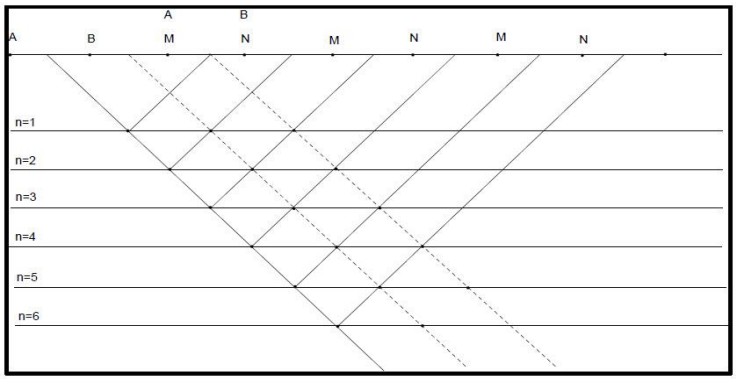

Figure 7: dipole-dipole array method.

A total of 10 geophysical profiles, comprising 7366 data points, were strategically positioned to delineate paleo-drainage networks and subsurface cultural horizons to a maximum depth of 20 m. These transects were established in coordination with the archaeological test trenches used for the delimitation of the core and buffer zones. Geophysical data acquisition at Tal-e Malyan utilised a combined Induced Polarisation and Electrical Resistivity (IP-ER) system. The survey covered a cumulative profile length of 2694 m, providing a comprehensive subsurface assessment of the site's geomorphological and anthropogenic features up to a depth of 20 m (Fig.4).

Results

Evidence Proving the Existence of a River in Tal-e Malyan

Based on preliminary field surveys, Trenches 9 and 18 were identified as key stratigraphic loci due to the presence of diagnostic fluvial deposits. These trenches serve as the primary proxy for reconstructing the paleohydrological dynamics and riverine proximity to Tal-e Malyan. Below is a detailed sedimentological characterisation of these sequences.

Trench 18

Trench 18 (1×1 m) was excavated to a depth of 325 cm, revealing a tripartite stratigraphic sequence composed of 13 distinct layers. The basal units are characterised by light grey lacustrine sediments that contain freshwater gastropods (Melanopsis sp.), indicating a low-energy lake environment. In contrast, the upper horizons exhibit signs of anthropogenic influence, transitioning to light yellowish-brown and yellow hues. A recurrence of light grey sediments was observed above the 100 cm mark. Notably, the horizon at a depth of 80 cm consists of concentrated hearth ash, indicative of localised combustion features associated with food processing or pyrotechnological activities. A total of 14 samples were recovered for high-resolution sedimentological analysis.

Granulometric analysis of Trench 18 (Table 2, Fig.8) reveals significant textural variability across the stratigraphic profile. The clay fraction ranges from a minimum of 2.18% (Sample 14) to a maximum of 27.5% (Sample 13). Silt content exhibits the widest fluctuation, peaking at 59.35% (Sample 4) while dropping to a negligible 0.23% in Sample 6. The sand fraction varies between 4.76% (Sample 14) and 33.3% (Sample 10). Notably, Sample 14 represents a high-energy depositional event, characterised by the maximum gravel content (89.53%) and a peak clast diameter of 75 mm. In contrast, Samples 4, 10, and 13 contain no gravel (0%), indicating lower-energy depositional conditions.

Table 2: Physical characteristics of Trench 18.

Sample	Colour	Clay (percent)	Silt (percent)	Sand (percent)	Gravel (percent)	Deposite Environment	Texture
T18-1	Light yellowish brown	23.81	58.55	15.63	1.99	IX	(g) sM
T18-2	Light grey	26.93	53.68	18.20	1.17	IX	(g) sM
T18-3	Light brownish grey	19.07	30.16	19.62	31.12	III	mG
T18-4	Light grey	26.6	59.35	14.05	0	VIII	sZ

T18-5	Light grey	10.00	11.10	19.31	59.57	I	mG
T18-6	-	2.43	0.23	15.51	81.82	I	G
T18-7	Light yellowish brown	6.27	5.66	22.14	65.92	I	msG
T18-8	Yellow	25.13	39.54	29.81	5.51	III	gM
T18-9	Pale yellow	9.38	10.28	20.45	59.87	I	msG
T18-10	Pale yellow	26.8	39.9	33.3	0	VI,VII	sM
T18-11	Light yellowish brown	5.93	6.83	13.60	73.62	I	msG
T18-12	Pale yellow	19.87	29.18	25.10	25.82	III	gM
T18-13	Light grey	27.5	43.8	28.7	0	III	sM
T18-14	Light grey	2.18	3.50	4.76	89.54	I	G

The sedimentary sequence in Trench 18 is characterised by a predominance of gravel and gravelly mud textures. Based on their textural maturity and clast size, Samples 14 and 6 are interpreted as in-channel facies, representing high-energy fluvial deposition. Conversely, Samples 5, 8, 9, 11, and 12 are attributed to episodic overbank flooding events, during which finer-grained gravelly muds were deposited due to increased discharge.

Depositional Environment I is identified within Samples 5, 6, 7, 9, 11, and 14 of Trench 18. This facies is characterised by coarse-grained clastics, with sediment transport primarily dominated by high-energy bed load and traction processes. In contrast, Sample 4 is associated with an anthropogenic combustion feature (Hearth VIII).

Granulometric parameters show significant variance across the profile. The mean grain size ranges from a maximum of 2250.79 µm (Sample 14) to a minimum of 9.38 µm (Sample 4). The sorting coefficients peaked in Sample 12 (17.73), indicating extremely poorly sorted deposits with high sediment homogeneity across layers. Conversely, Sample 6 exhibited the lowest sorting value (1.30), reflecting a concentrated distribution where over 80% of the sediment constitutes the gravel fraction. Skewness values varied between 0.08 (Sample 8) and -6.41 (Sample 6). Kurtosis analysis revealed a diverse range of distribution types: Samples 3, 6, 10, 12, and 14 are classified as very platykurtic; Samples 1, 2, 4, 8, and 11 are classified as platykurtic; and Samples 5 and 9 are classified as mesokurtic. Notably, Samples 7 and 11 demonstrated very to extremely leptokurtic distributions, suggesting highly focused depositional energy.

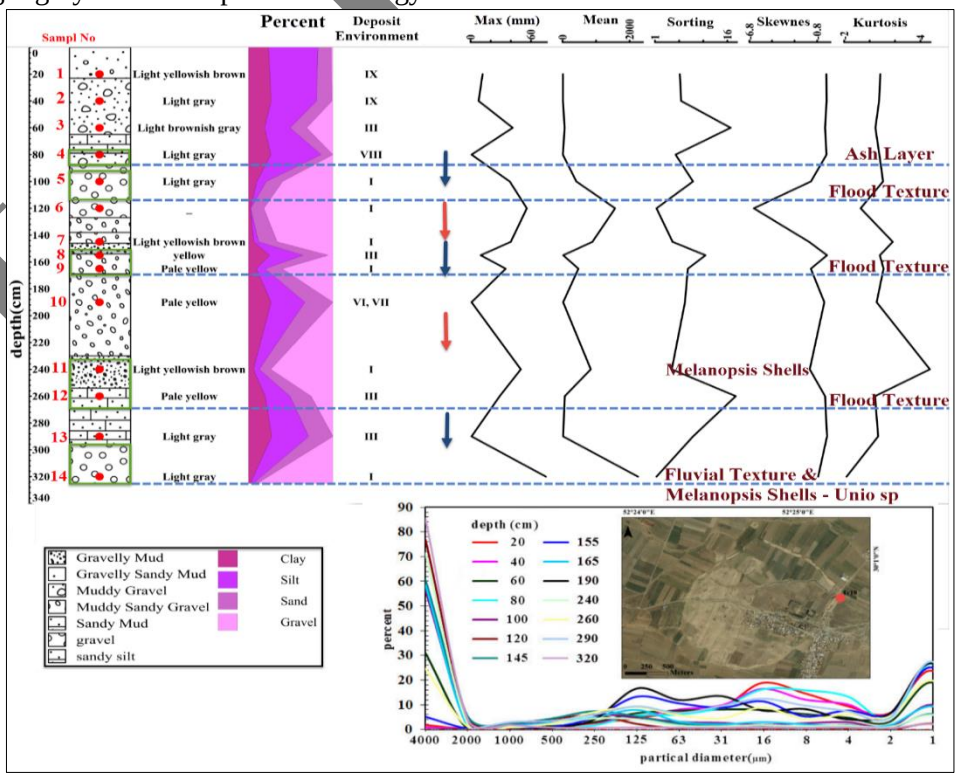

Figure 8: Physical characteristics of the sediments in Trench 18. (After: Google Earth 15/06/2024)

Trench 9

Trench 9 (1×2 m) was excavated to a depth of 140 cm in the southern sector of the site, revealing a natural stratigraphic sequence devoid of anthropogenic features. The profile consists of three primary layers from which four samples were recovered. The basal units exhibit reddish to brownish-yellow hues, transitioning to a distinct yellow chroma in the upper horizons. These colour variations, coupled with the soil morphology, indicate prevailing oxidising conditions within the sedimentary matrix, likely resulting from prolonged subaerial exposure or fluctuating water tables.

Granulometric analysis of Trench 9 (Table 3, Fig.9) reveals a significant textural gradient across the stratigraphic profile. The clay fraction peaks at 22.70% in Sample 1, decreasing to a minimum of 4.43% in Sample 4. A similar trend is observed in the silt content, which reaches a maximum of 48.54% (Sample 1) before dropping to a negligible 0.49% in Sample 4. Conversely, the sand fraction remains relatively stable, fluctuating between 13.03% (Sample 2) and 19.42% (Sample 3). The gravel component dominates the lower portion of the sequence, with Sample 4 exhibiting the highest concentration at 78.06% and a maximum clast diameter of 53 mm. In contrast, Sample 1 contains the least gravel fraction at 14.64%, indicating a transition toward a lower-energy depositional environment.

Table 3: Physical characteristics of Trench 9.

Sample	Colour	Clay (percent)	Silt (percent)	Sand (percent)	Gravel (percent)	Deposite Environment	Texture
T9-1	yellow	22.70	48.54	14.10	14.64	IX	gM
T9-2	yellow	18.24	28.64	13.03	40.07	II	mG
T9-3	Brownish yellow	11.80	11.37	19.42	57.39	I	mG
T9-4	Reddish yellow	4.43	0.49	17.01	78.06	I	msG

The sedimentary matrix is primarily composed of muddy gravel. A distinct fining-upward trend is observed, characterised by a progressive decrease in coarse-grained clastics from the basal units toward the surface horizons. Based on their textural properties and stratigraphic position, Samples 3 and 4 are interpreted as overbank splay deposits associated with high-magnitude flooding events.

According to the granulometric classification, Samples 3 and 4 are categorised under Environment I, while Samples 2 and 1 correspond to Environments II and IX, respectively. Analysis of the transport mechanisms within Trench 9 reveals significant dominance of traction load in the basal units, which progressively attenuates in the upper stratigraphic horizons. Nevertheless, traction-dominated flow remains the prevailing depositional regime throughout the profile, signifying sustained high-energy fluvial dynamics during the formation of these successions.

Statistical analysis of grain-size distribution reveals that the mean particle diameter peaks in Sample 4 (1481.83 μm) and reaches its minimum in Sample 1 (27.95 μm). Regarding the sorting coefficient, Sample 2 exhibits the highest degree of dispersion (15.78 μm), reflecting high sediment homogeneity across the stratigraphic layers. Conversely, the lowest sorting value was recorded in Sample 4 (1.70 μm), a result of the extreme concentration of over 78% of the sediment within the gravel fraction.

The skewness values for the samples range from 0.29 μm (Sample 1) to 2.80 μm (Sample 4). Overall, there is a general predominance of platykurtic distributions throughout the sequence. Notably, the strongly negative skewness of 2.57 μm in Sample 4 confirms a truncated distribution that is dominated by coarse-grained clastics, which is characteristic of high-energy fluvial transport.

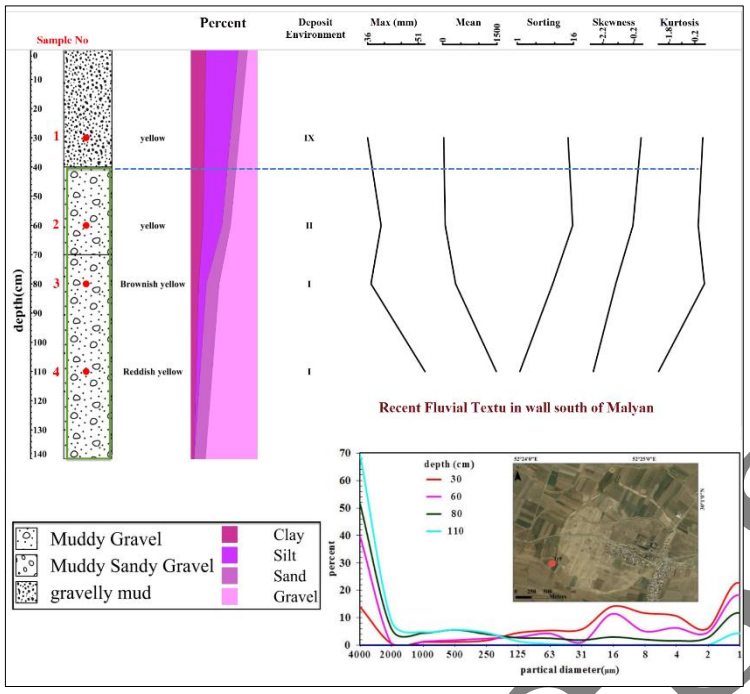

Figure 9: Physical characteristics of the sediments in Trench 9 (After: Google Earth 15/06/2024).

Physical Characteristics of Sediments

Principal Component Analysis (PCA) was employed to identify patterns in grain-size parameters after Z-score standardisation. All statistical analyses and graphical outputs were conducted using the R software environment. The first two components together explain 71.5% of the total variance, with PC1 and PC2 accounting for 45.7% and 25.8%, respectively. This indicates that a two-dimensional PCA effectively represents the dataset. Due to its high explained variance and strong loadings of grain-size variables, PC1 is interpreted as a proxy for depositional energy, where positive scores reflect high-energy conditions while negative scores indicate low-energy environments. Overall, the results demonstrate that grain-size variability in the study area is primarily governed by depositional energy, with PC1 serving a crucial role in differentiating between contrasting hydrodynamic regimes (Fig.10).

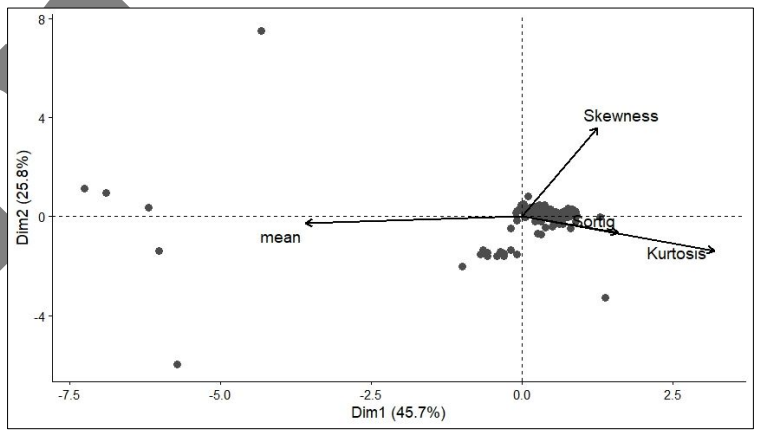

Figure 10: PCA biplot illustrating the relationships between grain-size parameters.

Figure 11 delineates the sediment classification based on granulometric distribution. The sedimentary matrix exhibits significant spatial variability: anthropogenic horizons in the northern sector (Trench 22) are predominantly gravelly mud, while the northeastern periphery (Trenches 17 and 19) yields a composition of mud and gravelly mud. In contrast, the northwestern area (Trench 23) is characterised

by sandy silt. The southern and southeastern sectors (Trenches 12, 14, and 24) transition into gravelly and sandy mud, a texture that also recurs in the northeastern reaches of the site (Trench 1).
The textural distribution of natural sedimentary sequences across the site exhibits marked lithological heterogeneity. In the northern and northwestern sectors, the matrix varies from sandy and gravelly mud (Trench 6) to high-energy muddy gravel (Trench 7). The northeastern area (Trenches 2 and 18) features a complex succession of mud, gravelly mud, and clast-supported gravel. Conversely, the eastern and southeastern zones (Trenches 15, 16, 20, 25, 26, and 27) are dominated by lower-energy deposits, including silt, sandy mud, and slightly gravelly mud. The western transect (Trenches 8, 9, and 11) displays the highest textural diversity, encompassing sandy mud and muddy gravel to poorly sorted gravelly facies. Lastly, the southwestern periphery (Trench 10) is mainly composed of gravelly mud, while specific northern pockets (Trench 19) exhibit finer-grained silt and mud successions.
Sedimentological analysis across the excavated transects reveals the presence of high-magnitude overbank flood facies within the upper stratigraphic units of Trenches 8, 9, 10, 12, 14, and 18. The presence of allochthonous ceramic fragments entrained within these flood deposits along the eastern periphery suggests significant high-energy fluvial impacts on pre-existing anthropogenic horizons. Regarding textural maturity, the anthropogenic samples are classified as immature, which are characterised of distal, extra-channel environments. These deposits contain clay concentrations exceeding 5%, exhibit poor sorting coefficients, and have a high frequency of angular clasts and fractured debris. Clay content within these cultural matrices ranges from 6.99% (Trench 1) to a peak of 36.8% (Trench 24). In contrast, natural sedimentary sequences reflect a broader range of sub-environments, from high-energy in-channel facies to low-energy floodplains. Specifically, the diminished clay fractions observed in Trenches 18 (2.18%), 9 (4.43%), and 11 (4.5%) are indicative of channel-core sub-environments, while the maximum clay enrichment (49% in Trench 20) signifies a stable, low-energy lacustrine or distal floodplain setting.

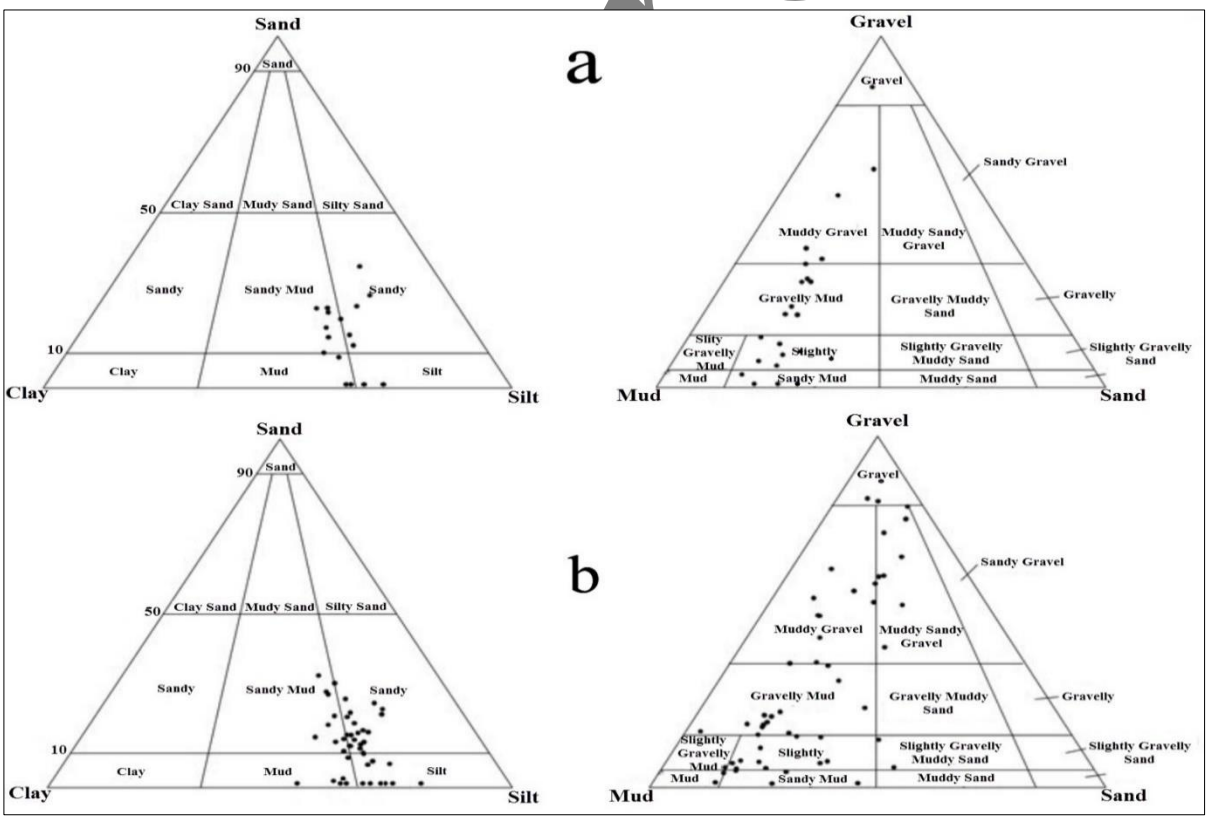

Figure 11: Classification of the sediments based on particle size. a. Samples of cultural texture trenches, b. Samples of natural texture trenches (After: Folk and Ward, 1957).

Sedimentary Environments and Evidence Related to Environmental Changes in Tal-e Malyan

The sedimentary successions at Tal-e Malyan reveal a dynamic transition between fluvial and lacustrine depositional environments. High-energy fluvial facies were predominantly identified in Trenches 8, 9, 11, and 18, characterised by a coarse-grained clastic matrix ranging from muddy gravel and gravelly mud to muddy sandy gravel.

The delineation of a stable lacustrine phase is primarily supported by malacological proxies recovered from Trench 18 (Fig.12). Specifically, the presence of freshwater gastropods (Melanopsis sp.) at a depth of 325 cm, with shell-bearing horizons persisting between 240 and 325 cm, correlates with regional distributions of these taxa across Fars Province, including the Parishan and Maharlu basins (Samaei and Mansourian, 2013). Furthermore, the occurrence of Unio sp. in Trenches 3, 5, 6, and 18 provides critical evidence for the existence of a persistent, low-energy freshwater body that characterised the local hydrology prior to, or during, the site's anthropogenic occupation phases.

Figure 12: Unio species and Melanopsis sp shells in Trench 18.(After:20/06/2023)

Geomorphological evidence suggests that a lacustrine regime predated the initial settlement phases at Tal-e Malyan. This interpretation is supported by the palaeotopography of the site's eastern margin, which is characterised by a closed depression aligned along a NW–SE structural axis extending toward the Bakhtegan Lake basin. The natural landscape between the Marvdasht and Beyza plains, particularly the presence of playa-like saline pits following this same tectonic orientation, further corroborates the existence of a high-water stand or a relic lake system in the pre-settlement period (Fig.13).

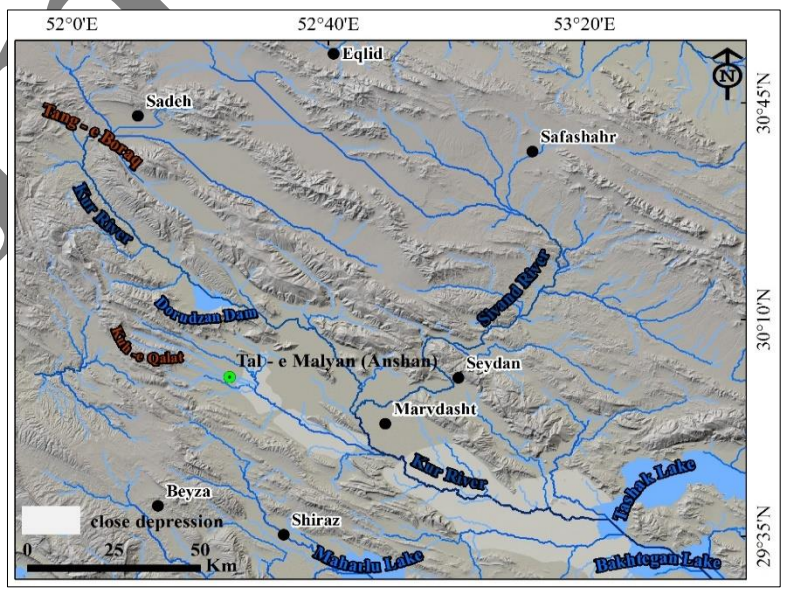

Figure ۱۳: Closed depression in the Bakhtegan basin (After: Sentinel 2 image - 20/07/2024).

The mean EC value (616.5 µS/cm) indicates that, on average, the soils in the study area fall well within the non-saline class (<2000 µS/cm). The median EC (400 µS/cm) is substantially lower than the mean, suggesting a right-skewed distribution influenced by a limited number of high EC values. The interquartile range (IQR = Q3 − Q1 = 332.5 µS/cm) confirms that 50% of the samples are concentrated within a relatively narrow EC range, reinforcing the dominance of low-salinity soils. The high coefficient of variation (CV = 96.8%) reflects significant spatial variability in soil salinity. In standard soil variability classifications, CV values exceeding 75% indicate high heterogeneity, suggesting that soil salinity is governed by localised pedogenic and environmental controls rather than uniform regional processes. This variability is typical of arid to semi-arid soilscapes, where micro-topography, differential leaching, evaporative salt accumulation, and drainage conditions strongly influence EC distribution. Although the majority of samples exhibit EC values below 1000 µS/cm, a small number of samples exceed 2000 µS/cm, with some reaching as high as 4500 µS/cm. These high values significantly elevate the overall standard deviation and mean EC, highlighting the presence of localised salinity hotspots (Table 4, Figure 14).

Table 4: Electrical conductivity (EC) values in Tal e- Malyan.

Sample	EC	Sample	EC	Sample	EC	Sample	EC	Sample	EC
T1-1	۳۴۳۰	T1-2	۱۰۱۰	T1-3	۱۲۶۰	T1-4	۵۸۰	T1-5	۷۹۰
T1-6	۴۷۰	T1-7	۴۰۰	T1-8	۳۹۰	T2-1	۴۲۰	T2-2	۴۲۰
T2-3	۴۳۰	T2-4	۱۷۳۰	T2-5	۱۸۸۰	T2-6	۱۰۴۰	T2-7	۱۷۶۰
T2-8	۱۳۹۰	T2-9	۱۱۶۰	T2-10	۲۰۷۰	T6-1	۳۴۰	T6-2	۳۰۰
T6-3	۲۹۰	T6-4	۳۶۰	T6-5	۳۷۰	T6-6	۲۹۰	T6-7	۲۸۰
T6-8	۲۸۰	T6-9	290	T6-10	370	T7-1	2840	T7-2	660
T8-1	250	T8-2	310	T8-3	240	T8-4	220	T8-5	220
T8-6	300	T8-7	480	T8-8	390	T9-1	350	T9-2	510
T9-3	740	T9-4	690	T10-1	550	T10-2	300	T10-3	540
T10-4	430	T10-5	460	T10-6	370	T11-1	450	T11-2	380
T12-1	370	T12-2	270	T12-3	700	T12-4	810	T12-5	490
T12-6	350	T12-7	320	T14-1	420	T14-2	770	T14-3	420
T14-4	450	T14-5	370	T14-6	310	T14-7	350	T14-8	330
T14-9	340	T14-10	330	T15-1	350	T15-2	390	T15-3	1100
T15-4	930	T15-5	800	T15-6	760	T16-1	840	T16-2	520
T16-3	480	T16-4	670	T16-5	470	T16-6	1150	T16-7	1040
T17-1	370	T17-2	370	T17-3	380	T17-4	540	T17-5	420
T17-6	330	T17-7	370	T17-8	360	T18-1	580	T18-2	1070
T18-3	320	T18-4	300	T18-5	310	T18-6	210	T18-7	300
T18-8	310	T18-9	320	T18-10	280	T18-11	290	T18-12	270
T18-13	260	T18-14	300	T19-1	690	T19-2	510	T19-3	530
T19-4	400	T19-5	530	T19-6	470	T19-7	440	T19-8	440
T20-1	1060	T20-2	2170	T20-3	4500	T20-4	1870	T20-5	1210
T20-6	650	T22-1	450	T22-2	770	T23-1	290	T23-2	350
T23-3	1570	T24-1	400	T24-2	330	T24-3	330	T24-4	280
T24-5	270	T24-6	270	T25-1	450	T25-2	490	T25-3	320
T25-4	310	T25-5	310	T26-1	340	T26-2	300	T26-3	430
T26-4	540	T27-1	380	T27-2	300	T27-3	390	T27-4	330

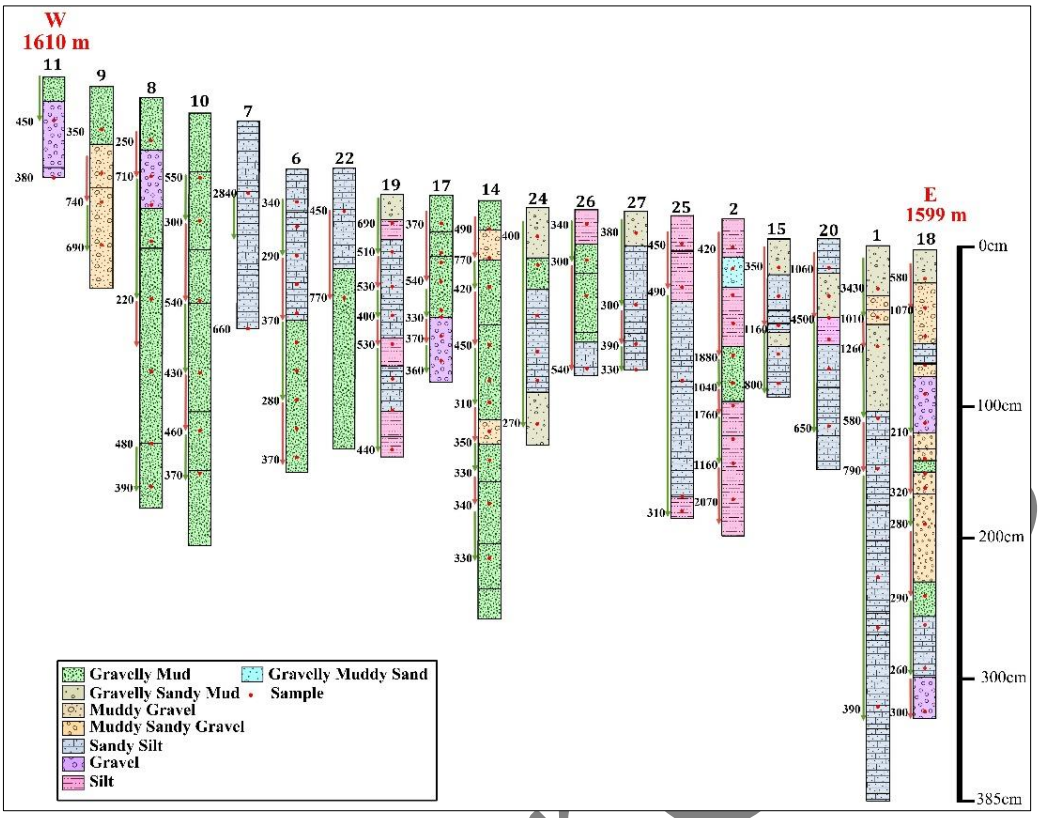

Figure 14: Electrical conductivity (EC) values in Tal e- Malyan.

Consequently, a marked increase in electrical conductivity (EC), exceeding 1000 µS/cm within the study area, signifies the onset of aridification and the subsequent regression of the lacustrine environment. This hydrological shift is stratigraphically evidenced by the presence of an evaporitic white horizon, which reflects intense evaporative processes under drying conditions. These data suggest a successional transition: the formation and eventual regression of a lake system that predated the Malyan occupation, followed by the establishment of an active drainage network concurrent with the period of human settlement (Fig.15).

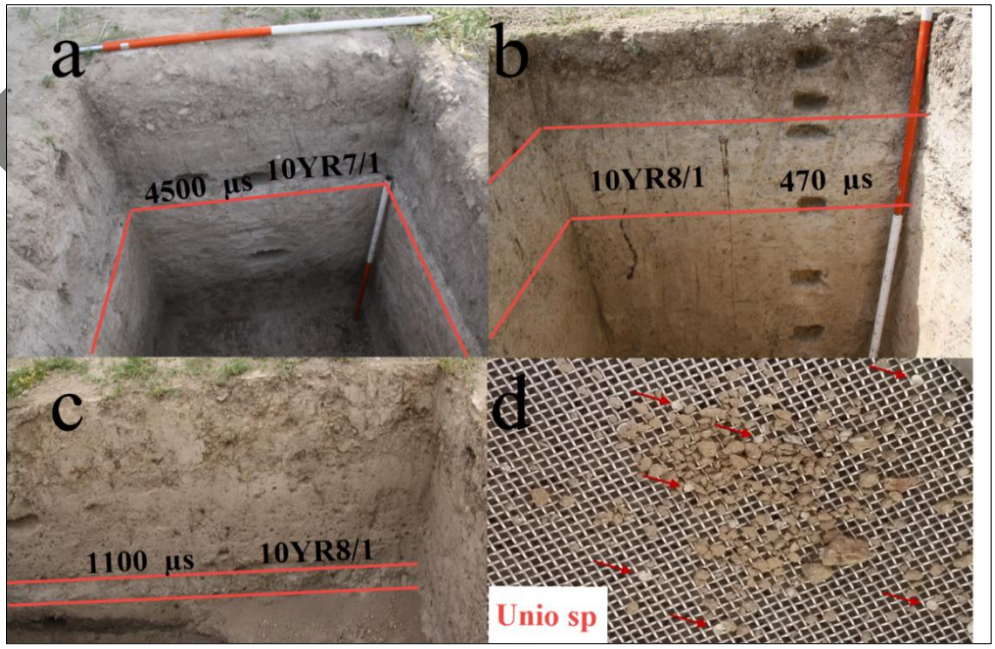

Figure 15: Unio species (Trench 2) and white layers in trenches at the eastern part of Tal-e Malyan (a: Trench 20, b: Trench16, c: Trench 15)(After:20/06/2022).

Geoelectric

The integrated stratigraphic and geophysical datasets reveal a complex palaeodrainage network intersecting the site, primarily documented within the sequences of Trenches 9 and 18. Based on distinct variations in channel morphology, width, and sedimentation rates, these fluvial systems are attributed to two chronologically discrete phases. The earlier network appears to have entered the site perimeter between Trenches 7 and 8 in the western sector, exiting through the northeastern quadrant at Trench 18. The presence of entrained ceramic fragments within the high-energy facies of Trench 18 confirms that this hydrological system was active during the sedimentary aggradation phases contemporaneous with the Tal-e Malyan settlement. Notably, the maximum clast diameters recorded in Trench 18 suggest that the residents occupied a landscape characterised by active, high-energy fluvial transport mechanisms, which directly influenced the site's spatial organisation and depositional history (Fig.16).

Figure 16: Coarse-grained sediments utilised in the foundation of structures at the ABC operation (After: Sumner, 2003: 340)

Geomorphological signatures of the palaeochannel remain discernible in the extramural areas of the site. In contrast, the intramural continuity of these fluvial features has been obscured by intensive anthropogenic modifications and the systematic extraction of alluvial aggregates during various occupation phases. Despite this stratigraphic hiatus within the site core, the spatio-temporal distribution of sediment fractions, coupled with diagnostic flood facies identified in Trenches 10 and 12 (downstream of Trench 9), corroborates a high-energy, west-east fluvial trajectory across the southern sector of the settlement.

Electrical Resistivity Tomography

Geophysical surveys, specifically electrical resistivity tomography (ERT), were executed along transects totalling 2694 metres across various sectors of Tal-e Malyan (Fig.17). These investigations were designed to delineate palaeochannel geometries and provide high-resolution subsurface data to corroborate and extend the findings of the granulometric and stratigraphic analyses.

Geophysical Profile 1, oriented NW–SE, was surveyed along the northern site exterior within current agricultural lands. The ERT data revealed significant resistivity peaks (≈100 Ω.m) within the near-surface horizons across three distinct sections. These anomalies correlate with coarse-grained clastic deposits identified in a control well located 70 m from the transect. Profile 3, oriented NE–SW, intersected Trenches 1 and 18 along the eastern fortification boundary. The upper 10 m of this section is characterised by high-resistivity anomalies, contrasting sharply with the basal units where resistivity drops below 20 Ω.m, indicating a transition to fine-grained, moisture-retentive sediments. Profile 10, conducted with a NE trend from the northern wall, displays an initial segment with a resistivity increase diagnostic of relic fluvial conduits. Profiles 5 and 6 cross the width of the northern wall, where substantial archaeological remnants persist. Although the resistivity signature suggests a wall width of 40 m, this is interpreted as the lateral extent of taphonomic collapse (wall tumble) rather

than the original structural thickness. Concentric high-resistivity anomalies detected exterior to the northern wall likely represent extramural fortifications or historical suburban features. In the western sector, Profile 7 (NE–SW) covered the EDD operation and Trench 8. Surface low-resistivity zones (rendered in blue) correspond to anthropogenic disturbance and backfilled excavation units. Beneath these, a distinct layer (≈50 Ω.m, rendered in brown) represents the preserved historical matrix of Malyan. Profile 8 (NE–SW) extends from the southern agricultural exterior, across the southern wall, to the central asphalt road. This transect intersected Trench 9 and the A63 operation (Sumner's excavations). The foot of the southern wall is marked by a 100 Ω.m anomaly, which persists across the wall's collapsed debris and aligns with the sedimentary signatures identified in Trench 11.

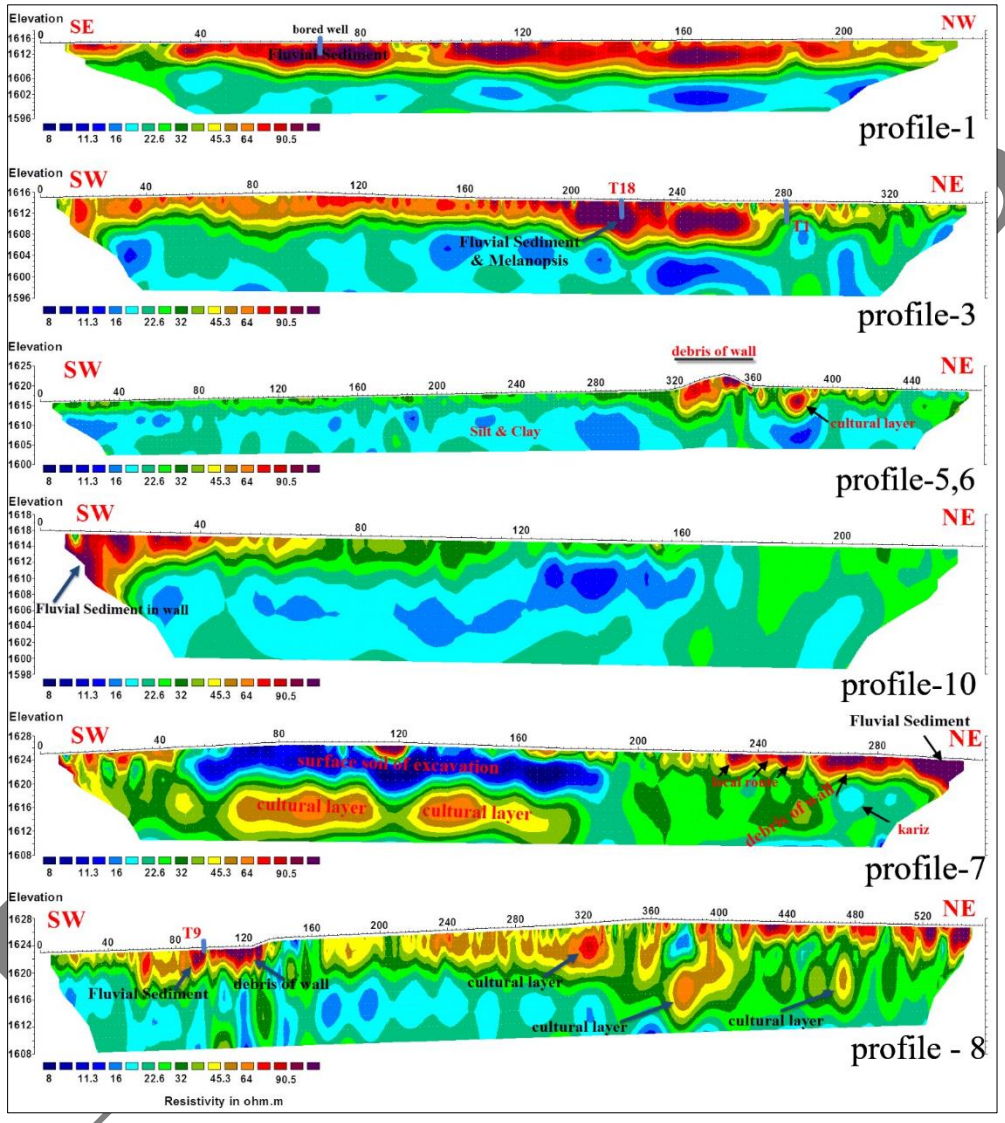

Figure 17: Resistivity Profile in Tal-e Malyan.(After:20/06/2022)

Discussion

The spatial distribution of archaeological sites in the Kur River basin, especially prior to the Banish Phase, was primarily concentrated along the river margins. Most settlements located on the western bank of the Kur River (Sumner, 1974: 157). However, Tal-e Malyan stands out as the most prominent and extensively documented site in the basin. It is characterised by substantial defensive fortifications that encompasses a perimeter of 5 km and cover an area of 200 ha (Sumner, 1985: 153). These fortifications were likely constructed to protect the settlement from nomadic and pastoral groups, as no other contemporaneous settlement within the Kur River basin was comparable in size or posed a similar threat to Tal-e Malyan's stability (Alden, 2013: 228).

During the Middle Banish Phase, Tal-e Malyan served not only as an urban centre but also as the largest permanent settlement in the region during that period (Petrie et al., 2009: 189). From a geomorphological perspective, the site was established on alluvial plain deposits, which provided favourable conditions for both agricultural production and pastoral activities. Water resources were supplied through a drainage network originating in the western highlands. A major channel identified in the northern sector of the site measures approximately 20 m in width and 6 m in depth. The presence of coarse sediments with a maximum particle diameter of 75 mm indicates a sustained and reliable water flow, sufficient to meet the needs of the settlement.

This evidence corresponds with broader regional patterns observed during the Early Banish Phase, marked by the abandonment of extensively occupied areas within the Kur River basin and the concentration of permanent settlements in the most humid parts of the region, including Tal-e Malyan. This shift suggests that rain-fed agriculture became increasingly unreliable over time (Alden, 2013: 225). In addition to the channel identified through geoelectrical surveys within the site, a series of enclosed depressions east of Tal-e Malyan have been documented. During wetter climatic phases, these depressions would have retained water, forming a lacustrine landscape along the eastern margin of the settlement.

Sumner documents a progressive reduction in settlement area from the early fourth millennium BCE (end of the Bakun Phase) to the late third millennium BCE (beginning of the Kaftari Phase). This trend is interpreted as the result of a long-term decline in the productivity of the regional agricultural system, primarily driven by soil salinisation. Such environmental degradation ultimately led to a restructuring of the regional economy, shifting from agriculture toward a Banesh-period economic system that increasingly oriented toward pastoralism and nomadic lifeways (Sumner, 1986: 209). During the final phase of occupation at Tal-e Malyan, a marked transition toward more arid environmental conditions is evident, particularly in the eastern sectors of the site (Fig. 15).

Conclusion

The Tal-e Malyan site, covering an area of 200 hectares and dating back to 5200 BP, has been continuously inhabited and is regarded as one of the most significant cities of the Middle Elamite period. Numerous archaeological investigations have been carried out at the site, all conducted by specialised archaeological teams. However, a notable gap in previous research was the absence of geoarchaeological studies, which began in 2017 following the delineation of the site's core area and buffer zone. These studies marked the commencement of the first geoarchaeological investigations at Tal-e Malyan. The primary aim of this study was to address the five key questions outlined in the introduction, which are summarised as follows:

The location of Tal-e Malyan was significantly influenced by its environmental conditions. The presence of a drainage network originating from the western highlands (Kuh-e Qalat) provided a consistent and reliable water source for the settlement. In contrast, the central parts of the Kur River basin, with shallow depressions and lakes, were not suitable for long-term settlement. However, the western part of the basin offered more favourable living conditions. Regarding environmental dynamics, the central portion of the Kur River basin was primarily characterised by a riverine system, while the eastern section of the site was periodically affected by the formation of shallow lakes during wet periods. These lakes formed intermittently, typically at short distances from one another. Analysis of the environmental changes recorded in the site's sediments revealed three wet periods and two dry periods, during which the river regime shifted to a flood-dominated system in the dry intervals (Fig.8). Previous studies at Tal-e Malyan did not include references to a drainage network, but geoelectrical results have provided clear evidence of the presence of river channels. The source of the drainage system at the site is the western highlands (Kuh-e Qalat), which are predominantly composed of the Asmari and Gurpi formations.

A notable challenge at Tal-e Malyan is the presence of a wall and embankment, approximately 5 metres in height, with remnants found in the northern and northeastern areas of the site, dating back to 4600 BP (Sumner, 1985). From a natural perspective, erosional processes have not possessed sufficient power to dismantle or erode this substantial structure, as evidenced by the sediment size in Trench 9 and the upper layers of Trench 18. According to Sumner (1985:153), the southern section of

the wall was likely destroyed by subsequent agricultural activities. Consequently, it appears that this protective wall was primarily destroyed by non-natural factors, with subsequent natural processes gradually accelerating its deterioration over time.

Acknowledgment

This study was supported by the Iranian Centre for Archaeological Research (ICAR) and the Geological Survey and Mineral Exploration of Iran. The authors gratefully acknowledge the efforts of these organisations.

References

- Abdi, K. (1999). Archaeological research in the Islamabad plain, central western Zagros Mountains: preliminary results from the first season, summer 1998. Iran, 37(1), 33-43.
- Adameková, K., Prišťáková, M., Doláková, N., Dresler, P., Nehyba, S., Dlapa, P., ... & Světlík, I. (2025). Soil-alluvial dynamics, landscape evolution, and human activity in the Thaya river floodplain (Czech Republic) from the Late Pleistocene to the Holocene. Quaternary Science Advances, 19, 100287.
- Aguilar, R. G., Owens, R., & Giardino, J. R. (2020). The expanding role of anthropogeomorphology in critical zone studies in the Anthropocene. Geomorphology, 366, 107165.
- Alaei Taleghani, M. (2017). Geomorphology of Iran, Ghoomes Publishing Company.
- Alden, J. R. (1979). Regional Economic Organization in Banesh Period, Iran, University of Michigan (Doctoral dissertation, Ph. D. dissertation).
- Alden, J. R. (2013). 12. THE KUR RIVER BASIN IN THE PROTO-ELAMITE ERA–SURFACE SURVEY, SETTLEMENT PATTERNS, AND THE APPEARANCE OF FULL-TIME TRANSHUMANT PASTORAL. Ancient Iran and its Neighbours, 207.
- Aminpour, B. (2001). Application of exploratory geophysical methods in archaeology and an example of implementing magnetometry around the ChoghaZanbil Ziggurat, Archaeological Research Journal, N0. 8, 4-9.
- Bevan, B. W., & Smekalova, T. N. (2013). Magnetic exploration of archaeological sites. In Good Practice in Archaeological Diagnostics: Non-invasive Survey of Complex Archaeological Sites (pp. 133-152). Cham: Springer International Publishing.
- Biglari, F., Mashkour, M., Shidrang, S., Javeri, M., Yazdi, M., Tenberg, M., Bahrololumi, F., Darvish, J., Taheri, K. (2015). Qaleh Bozi, New Evidence of Late Middle Paleolitic Occupation in the Zayandeh –Rud Basin, Esfahan Province, PAZHOHESH-HA-YE BASTANSHENASI IRAN, Vol.4 No7.
- Blackman, M. J. (1981). The mineralogical and chemical analysis of Banesh period ceramics from Tal-e-Malyan, Iran. In Scientific Studies in Ancient Ceramics (Vol. 19, pp. 7-20). British Museum London.
- Brandolini, F., & Carrer, F. (2021). Terra, Silva et Paludes. Assessing the role of alluvial geomorphology for Late-Holocene settlement strategies (Po Plain–N Italy) through point pattern analysis. Environmental Archaeology, 26(5), 511-525.
- Chandel, P., Anand, S., & Singh, D. (2022). An overview of scientific research on geoheritage in India. Geoheritage, 14(4), 131.
- Dong, G., Liang, H., & Zhang, Z. (2024). Human–environment interaction along the eastern Silk Road during the Neolithic and Bronze Age. Palaeogeography, Palaeoclimatology, Palaeoecology, 649, 112340.
- Emmanuel, R., Alessia, P., & Paola, C. (2017). Urban Geomorphological Heritage. An Overview. Quaestiones Geographicae, 36(3), 7-20.
- Folk, R. L., & Ward, W. C. (1957). Brazos River bar [Texas]; a study in the significance of grain size parameters. Journal of Sedimentary Research, 27(1), 3-26.

- Gee, G. W., & Bauder, J. W. (1986). Particle-size analysis. Methods of soil analysis: Part 1 Physical and mineralogical methods, 5, 383-411.
- Ghilardi, M., Colleu, M., Pavlopoulos, K., Fachard, S., Psomiadis, D., Rochette, P., ... & Bicket, A. (2013). Geoarchaeology of ancient aulis (boeotia, Central Greece): human occupation and holocene landscape changes. Journal of Archaeological Science, 40(4), 2071-2083.
- Gibbard, P., Walker, M., Bauer, A., Edgeworth, M., Edwards, L., Ellis, E., ... & Ruddiman, W. (2022). The Anthropocene as an event, not an epoch. Journal of Quaternary Science, 37(3), 395-399.
- Gillmore, G. K., Stevens, T., Buylaert, J. P., Coningham, R. A., Batt, C., Fazeli, H., ... & Maghsoudi, M. (2011). Geoarchaeology and the value of multidisciplinary palaeoenvironmental approaches: a case study from the Tehran Plain, Iran. Geological society, london, special Publications, 352(1), 49-67.
- Goudie, A. (2020). The human impact in geomorphology–50 years of change. Geomorphology, 366, 106601.
- Hatswell, O., Moffat, I., Ames, C. J., Shaw, M., Phillips, N., McNeil, J. L., ... & Mackay, A. (2025). Understanding the Depositional History of the Archaeological Open-Air Site, Klein Hoek 1, South Africa, Using Geophysical Geoarchaeology. Geoarchaeology, 40(3), e70015.
- Herrera-Franco, G., Carrión-Mero, P., Montalván-Burbano, N., Caicedo-Potosí, J., & Berrezueta, E. (2022). Geoheritage and geosites: A bibliometric analysis and literature review. Geosciences, 12(4), 169.
- Heydari-Guran, S., Benazzi, S., Talamo, S., Ghasidian, E., Hariri, N., Oxilia, G., ... & Lahr, M. M. (2021). The discovery of an in situ Neanderthal remain in the Bawa Yawan rockshelter, west-central Zagros Mountains, Kermanshah. PloS one, 16(8), e0253708.
- Hill, Christopher. L., & Rapp, G. (2014). Geoarchaeology. In: Claire Smith, Encyclopedia of Global Archaeology, Springer New York, 3008–3017.
- Jefferson, A. J., Wegmann, K. W., & Chin, A. (2013). Geomorphology of the Anthropocene: Understanding the surficial legacy of past and present human activities. Anthropocene, 2, 1-3.
- Kharazian, M. A., Jamet, G., Puaud, S., Nasab, H. V., Hashemi, M., Guerin, G., ... & Berillon, G. (2022). First geoarchaeological study of a Palaeolithic site on the northern edge of the Iranian Central Desert: Mirak (Semnan, Iran). Journal of Arid Environments, 201, 104739.
- Khodabakhshi, S; Karimian Eghbal, M; Hejebri Nobari, A. (2012). Micromorphological Investigation of Iron Age Cemetery in Kabood Mosque Archeological Site Tabriz, Iran. A thesis presentd for the degree of Master of Science (M.SC).
- Liritzis, I., Westra, A., & Miao, C. (2019). Disaster geoarchaeology and natural cataclysms in world cultural evolution: An overview. Journal of Coastal Research, 35(6), 1307-1330.
- Lowe, J. J., & Walker, M. (2014). Reconstructing quaternary environments. Routledge.
- Lü, J., Mo, D., Zhuang, Y., Jiang, J., Liao, Y., Lu, P., ... & Feng, J. (2019). Holocene geomorphic evolution and settlement distribution patterns in the mid-lower Fen River basins, China. Quaternary international, 521, 16-24.
- Maghsoudi, M., Simpson, I.A., Kourampas, N., Fazeli Nashli, H. (2014). Archaeological sediments from settlement mounds of the Sagzabad cluster, central Iran: Human-induced deposition on an arid alluvial Plain, Quaternary International, 1-17.
- Maghsoudi, M., Zamanzadeh, S. M., Navidfar, A., Yosefi Zoshk, R., & Ahmadpour, H. (2015). Geoarchaeology of Prehistoric Settlements Using Micromorphology Methods (The case study: Meimanatabad Cluster). Journal of Archaeological Studies, 7(2), 149-164.

- Maurizio, L., & Silvestro, L. (2012). Geological and geomorphological hazard in historical and archaeological sites of the mediterranean area: knowledge, forecasting and mitigation. DISASTER ADVANCES, 5(3), 63-71.
- Miller, N. F. (1982). Economy and environment of Malyan, a third millennium BC urban center in southern Iran.
- Mofidi-Nasrabadi, B; Mirzaei, A. (2013). Stratigraphic studies in the ancient hill of Deh-e Nou (Khuzestan), Journal of Archaeological Studies, vol. 5 No 1.
- Mohammadkhani, K; Naif, S. (2018). The Introduction of the Archaeological Site of Sibeh-Koukherd, Based on Archaeological and Arcaeogeophysical Surveys Data, Journal of Research on Archaeometry, 4 (2):1 19.
- Naderi Beni, A., Lahijani, H., Tofighian, H., & Morshedloo, J. (2025). Geohistorical and geoarchaeological evidence of seafaring in the Caspian Sea: Lessons from the past to draw the future. Journal of Island and Coastal Archaeology, 20(4), 844-876.
- Nehybaková, S., Adameková, K., Doláková, N., Dresler, P., Petřík, J., & Přišťáková, M. (2023). Unraveling Mediaeval human traces in fluvial deposits of the Dyje River near the Pohansko stronghold (Czech Republic). Geological Quarterly, 67.
- Nicholas, I. M. (1980). A spatial/functional analysis of late fourth millennium occupation at the TUV mound, Tal-e Malyan, Iran.
- Pelfini, M., Brandolini, F., D'Archi, S., Pellegrini, L., & Bollati, I. (2021). Papia civitas gloriosa: Urban geomorphology for a thematic itinerary on geocultural heritage in Pavia (Central Po Plain, N Italy). Journal of Maps, 17(4), 42-50.
- Persico, L., Lanman, H., Loopesko, L., Bruner, K., & Nicolaysen, K. (2018). Geomorphic processes influence human settlement on two islands in the Islands of Four Mountains, Alaska. Quaternary Research, 1, 19.
- Petrie, C. A., Weeks, L., Potts, D. T., & Roustaei, K. (2009). Perspectives on the cultural sequence of Mamasani. In The Mamasani Archaeological Project Stage One: A report on the first two seasons of the ICAR-University of Sydney expedition to the Mamasani District, Fars Province, Iran (p. 169). Archaeopress.
- Prabhakar, B. C., & Radhika, K. N. (2022). Recognizing new geoheritage sites in Karnataka, India. Geoheritage, 14, 1-24.
- Quesada-Valverde, M. E., & Quesada-Román, A. (2023). Worldwide trends in methods and resources promoting geoconservation, geotourism, and geoheritage. Geosciences, 13(2), 39.
- Reiner, E. (1974). Tall-i Malyan, Epigraphic finds, 1971-72. Iran, 12, 176.
- Renfrew, C. (1972). The Emergence of Civilisation: The Cyclades and the Aegean in the Millennium BC. Methuen.
- Reynard, E., Pica, A., & Coratza, P. (2017). Urban geomorphological heritage. An overview. Quaestiones geographicae, 36(3), 7-20.
- Samadi, L. (2012). Basic applied Geophics, Iranian Students Booking Agency.
- Samaei, A & mansourian, A. (2013). Gastropoda of Iran. Gisa publication
- Sardari, A., Ahmadpour, H., Khanipour, M., Navidfar, A. (2019). Excavations at Tall-i Malyan (Anshan), Iranian Center for Archaeological Research (ICAR).
- Stolper, M. W. (1985). Proto-Elamite Texts from Tall-i Malyan. Kadmos, 24(1-2), 1-12.
- Sumner, W. M. (1972). Cultural development in the Kur River basin, Iran. An archaeological analysis of settlement patterns. University of Pennsylvania.
- Sumner, W. M. (1985). The proto-Elamite city wall at Tal-i Malyan. Iran, 23, 153-161.
- Sumner, W. M. (2003). Early Urban Life in the Land of Anshan: Excavations at Tal-e Malyan in the Highlands of Iran, Malyan Excavation Reports, Volume III.
- Sumner, W. M., & Finkbeiner, U. (1986). proto-Elamite civilization in Fars. Ğamdat Naṣr-period or regional style?, 199-211.

- Sumner, W., & Reiner, E. (1974). Excavations at Tall-i Malyan, 1971–72. Iran, 12(1), 155-180.
- Taheri, K., Mashkour, M., Biglari, F. (2007). Zilou Cave: A Karstic Shaft with Animal Bones at Kermanshah Region, Western Iran, The 11th Conference of Geological Society of Iran, Ferdowsi University of Mashhad, 3340 – 3348.
- Tarolli, P., Sofia, G., & Cao, W. (2018). The geomorphology of the human age. Encyclopedia of the Anthropocene, 1, 35-42.
- Topography map of Marvdash 1:25000, Iran National Cartographic Center (https://geo.gov.ir/).
- Tucker, M. E. (2003). Sedimentary rocks in the field. John Wiley & Sons.
- Waters, M. R. (1988). Holocene alluvial geology and geoarchaeology of the San Xavier reach of the Santa Cruz River, Arizona. Geological Society of America Bulletin, 100(4), 479-491.
- Woodward, J., & Huckleberry, G. (2011). The geoarchaeology of river basin systems: an introduction. Geoarchaeology, 26(5), 611-615.
- Xu, K., & Wu, W. (2022). Geoparks and geotourism in China: A sustainable approach to geoheritage conservation and local development—A review. Land, 11(9), 1493.
- Zeder, M. A. (1985). Urbanism and animal exploitation in southwest highland Iran, 3400-1500 BC (Doctoral dissertation, University of Michigan).
- Zielhofer, C., Rabbel, W., Wunderlich, T., Vött, A., & Berg, S. (2018). Integrated geophysical and (geo) archaeological explorations in wetlands. Quaternary International, 473, 1-2.